Available online at www.sciencedirect.com
SCIENCE DIRECT®
Earth and Planetary Science Letters 247 (2006) 171–184
EPSL
www.elsevier.com/locate/epsl

Magnesian anorthosites and a deep crustal rock from the farside crust of the moon

Hiroshi Takeda [a,*], A. Yamaguchi [b], D.D. Bogard [c], Y. Karouji [d], M. Ebihara [d], M. Ohtake [e], K. Saiki [f], T. Arai [b]

[a] *Research Inst., Chiba Inst. of Tech., 2-17-1 Tsudanuma, Narashino City, Chiba 275-0016, Japan*
[b] *National Inst. of Polar Research (NIPR), Itabashi-ku, Tokyo 173-8515, Japan*
[c] *ARES, Code KR, NASA Johnson Space Center, Houston, TX 77058, USA*
[d] *Department of Chemistry, Tokyo Metropolitan Univ., Hachioji, Tokyo 193-0397, Japan*
[e] *Planetary Science Department, Japan Aerospace Exploration Agency (JAXA), 3-1-1 Yoshinodai, Sagamihara, 229-8510, Japan*
[f] *Department of Earth and Space Science, Graduate School of Science, Osaka Univ., 1-1 Machikaneyama, Toyonaka 560-0043, Osaka, Japan*

Received 17 October 2005; received in revised form 31 March 2006; accepted 4 April 2006
Available online 9 June 2006
Editor: R.W. Carlson

Abstract

Among over thirty lunar meteorites recovered from the hot deserts and Antarctica, Dhofar 489 is the most depleted in thorium (0.05 ppm), FeO, and rare earth elements (REE). Dhofar 489 is a crystalline matrix anorthositic breccia and includes clasts of magnesian anorthosites and a spinel troctolite. The Mg/(Mg+Fe) mol% (Mg numbers=75–85) of olivine and pyroxene grains in this meteorite are higher than those of the Apollo ferroan anorthosites. Such materials were not recovered by the Apollo and Luna missions. However, remote sensing data suggest that the estimated concentrations of Th and FeO are consistent with the presence of such samples on the farside of the Moon. The differentiation trend deduced from the mineralogy of the anorthositic clasts define a magnesian extension of the ferroan anorthosite (FAN) trend constructed from the Apollo samples. The presence of magnesian anorthositic clasts in Dhofar 489 still offers a possibility that the farside trend with magnesian compositions is more primitive than the FAN trend, and may require a revision of this classical differentiation trend. The Ar–Ar age of Dhofar 489 is 4.23±0.034 Gyr, which is older than most Ar ages reported for highland rocks returned by Apollo. The old Ar–Ar age of impact formation of this breccia and the presence of a fragment of spinel troctolite of deep crustal origin suggest that a basin forming event on the farside excavated the deep crust and magnesian anorthosites before formation of Imbrium.

Keywords: lunar meteorite; anorthosite; lunar farside; spinel troctolite; magma ocean

1. Introduction

Clementine and Lunar Prospector remote sensing data indicate that the nearside and the farside of the Moon are substantially different in terms of inferred chemical composition and rock lithologies [1–3].

* Corresponding author. Tel./fax: +81 47 478 0420.
E-mail address: takeda.hiroshi@it-chiba.ac.jp (H. Takeda).

0012-821X/$ - see front matter © 2006 Elsevier B.V. All rights reserved.
doi:10.1016/j.epsl.2006.04.004

Several incompatible trace elements (e.g., Th, U) are concentrated within and around the Procellarum KREEP Terrain (PKT) [3], the origin of most returned Apollo samples. One Dhofar lunar meteorite reported recently [4] was proposed to come from the most Th-rich region in the PKT. Ferroan anorthosites (FAN) have long been known to be a major rock type in the lunar highlands and are thought to be remnants of early lunar differentiation [3,5]. However, large regions of the lunar surface, particularly the northern farside highlands, are low in FeO and Th. Some lunar meteorites have been proposed to represent a type of highland materials with lesser amounts of FeO and Th than those of the breccias of the PKT, but a proposal that such lunar meteorites represent the low-FeO, low-Th highlands is not yet accepted [6,7]. Highland materials originating from the low-FeO, low-Th region on the farside of the Moon, as revealed in orbital data, are not represented in the Apollo collections. Dhofar 489, as we report in this paper, has very low FeO and Th compared to other lunar meteorites, and gives an older Ar–Ar age than most of the ferroan anorthosites. Therefore, it can be a representative sample of a rock-type of this farside region.

Pristine, non-mare, lunar rocks have plagioclase An values [Ca/(Ca+Na+K) mol%] and coexisting mafic mineral Mg numbers that are distributed along two trends [5] separated by a "gap." This differentiation trend is one of the well-known trends of the early magma ocean model of the Moon based on the Apollo samples. Now, many investigators think that Mg-suite rocks are related to later plutonism, not primary magma ocean igneous activity [8]. Some lithic clasts with granulitic textures in highland breccias from the PKT, along with some lunar meteorites, plot within the "gap" [9,10]. These investigators point out that granulites and granulitic breccias fall in the "gap", because they were originally breccias and do not accurately reflect igneous trends. The differentiation trend deduced from the mineralogy of the anorthositic clasts in Dhofar 489 starts at a more magnesian composition than the FAN trend.

2. Mineralogy–petrology of Dhofar 489

Dhofar 489 is a 34.4 g lunar rock, found in the hot desert of Oman [11]. It is a feldspathic breccia having feldspathic lithologies embedded into a much finer-grained, dark crystalline matrix (Fig. 1a). Subrounded mafic silicates are embedded in shocked plagioclases or recrystallized matrices. Five polished thin sections of Dhofar 489 were employed for mineralogical and petrographic studies. PTS1, made from a thin slice, was used to describe this breccia in the first report [11]. The largest chip at the National Science Museum in Tokyo (NSMT), $2.2 \times 1.6 \times 1.2$ cm^3 in size, showed a cut surface exposing a milky-white plagioclase clast

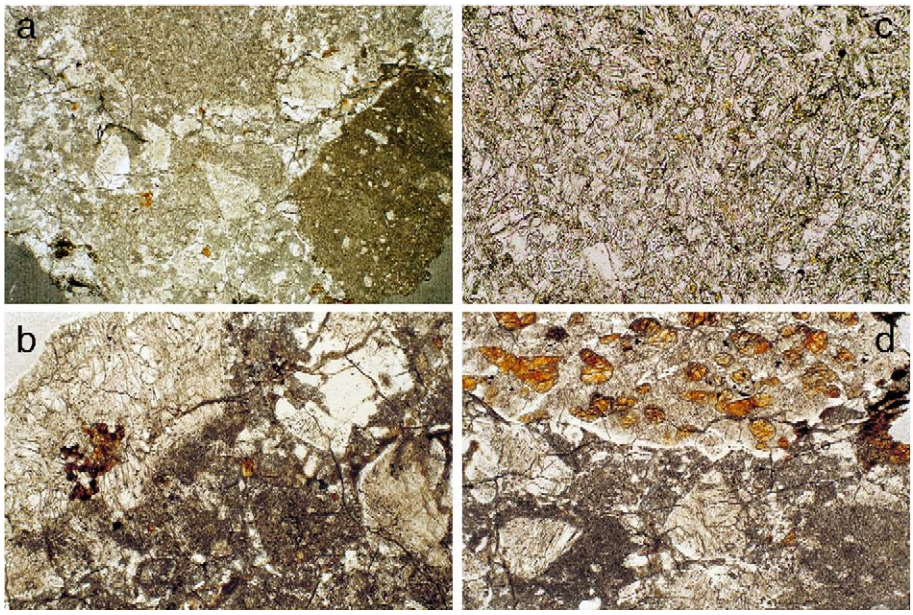

Fig. 1. Photomicrograph of PTSs of Dhofar 489: (a) an entire view of the crystalline matrix breccia, width=6 mm; (b) a magnesian anorthositic clast (upper left) with amoeboidal mafic silicates grains, width=3.3 mm; (c) a close-up view of the crystalline matrix, width=0.6 mm; (d) the spinel troctolite clast (top half), width=3.3 mm.

3.2×2.1 mm^2 in size and a grayish white clast 8.5×5.3 mm^2 in size. These portions were used for the trace element analysis and the Ar–Ar age dating. The second chip from the Japan Aerospace Exploration Agency (JAXA) includes a rock fragment of spinel troctolite and milky white anorthositic clasts in the crystalline matrix breccia. Three PTSs (11, 11-1 and 11-3) were made from this chip. PTS 2-1 was made from a chip at the National Institute of Polar Research (NIPR), and includes three lithic clasts.

Elemental distribution maps of Si, Mg, Fe, Al, Ca, Ti and Cr were obtained by electron probe microanalysis (EPMA) at the Ocean Research Institute (ORI) of the University of Tokyo and at NIPR. Modal abundances (vol.%) of minerals in some clasts were derived from these maps. Chemical compositions of minerals were analyzed by JEOL 733 EPMA at ORI. A beam diameter of 5 μm was used for the determination of alkali contents in plagioclases and glasses. Bulk chemical compositions of the crystalline matrix, melt breccia, and melt veins were obtained by averaging 9 points of broad beam (5 μm beam diameter) analyses and 20 to 40 points along line of 3 μm intervals.

Some parts of the matrix of PTS 1 have a much coarse-grained texture with fine, lath-shaped plagioclase crystals up to 0.05 mm in length (Fig. 1c). The boundaries between matrices and plagioclase fragments are not clearly defined. The matrix texture in other PTSs of the second chip are much finer (less than a few μm), and often fine, dusty, dark, crystalline materials are distributed even in the white anorthositc clasts. This material represents devitrification of maskelinite and is a clear indicator of shock metamorphism and annealing.

The bulk composition of the crystalline matrix is essentially anorthositic and contains lower FeO and MgO concentrations (FeO max=2.8 wt.%, mean=1.3 wt.%, MgO max=4.1 wt.%, mean=1.3 wt.%) than those of other lunar meteorites and of Apollo 16 anorthositic breccias and granulites. The dark crystalline material adjacent to a plagioclase clast contains FeO up to 7.7 wt.% and MgO=7.3 wt.%. PTS 1 includes a clast-laden, impact-melt breccia (IMB) clast (Fig. 1a, right side). The dark, devitrified matrix in the IMB is also anorthositic (FeO max=1.9 wt.%, mean=0.8 wt.%, MgO max=1.2 wt.%, mean=0.7 wt.%). An impact melt vein penetrating both clasts and matrix also has a similar bulk composition.

Mineral compositions of olivine and pyroxene grains (Table 1a) are more magnesian than common lunar feldspathic meteorites [6,10,11]. The forsterite (Mg_2SiO_4, Fo) content of all olivine grains in this meteorite (including grains in both matrix and clasts) has a bimodal distribution with peaks at Fo75–77 and Fo84–85 (Fig. 2). The largest olivine fragment (Fo71) in

Table 1a
Chemical compositions (wt.%) of major mafic minerals in Dhofar 489 lunar meteorite

	Spinel troctolite				Magnesian anorthosite		Fragments	
	Olivine	Opx [a]	Augite	Spinel	Oliv. gr [b]	Oliv. atch [c]	Olivine	Opx [a]
No. [d]	13	7	3	3	18	16	9	4
SiO_2	39.58	55.51	53.54	0.27	38.74	38.18	37.37	54.09
TiO_2	0.04	0.77	1.34	1.81	0.05	0.03	0.03	0.41
Al_2O_3	0.22	1.37	1.93	37.65	0.06	0.08	0.03	0.92
FeO	15.06	9.39	3.79	14.98	19.29	22.40	25.81	15.75
MnO	0.19	0.20	0.10	0.17	0.23	0.26	0.31	0.30
MgO	44.42	31.43	17.65	14.97	41.19	38.36	35.79	27.25
CaO	0.18	1.33	21.80	0.26	0.17	0.22	0.25	0.99
Na_2O	0.02	0.02	0.06	0.00	0.01	0.00	0.00	0.01
K_2O	0.01	0.02	0.02	0.00	0.01	0.01	0.00	0.02
Cr_2O_3	0.09	0.46	0.49	29.65	0.11	0.13	0.06	0.29
V_2O_3	0.01	0.03	0.03	0.15	0.01	0.01	0.01	0.04
NiO	0.03	0.06	0.02	0.02	0.04	0.02	0.02	0.01
P_2O_5	0.08	0.01	0.00	0.01	0.01	0.04	0.01	0.01
Total	99.91	100.58	100.76	99.94	99.91	99.75	99.71	100.05
Mg (Fo)	84.0	83.5	49.8		79.1	75.3	71.2	74.1
Fe (Fa)	16.0	14.0	6.0		20.9	24.7	28.8	24.0
Ca		2.5	44.2					1.9

[a] Orthopyroxene.
[b] Olivine with granulitic shape.
[c] Olivine attached at a corner of plagioclase clast.
[d] Numbers of measurements.

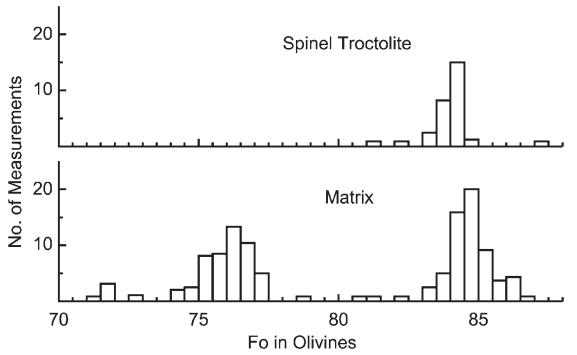

Fig. 2. Fo compositions of olivine crystals in the spinel troctolite (ST) clast and fragments in the matrices and clasts of Dhofar 489.

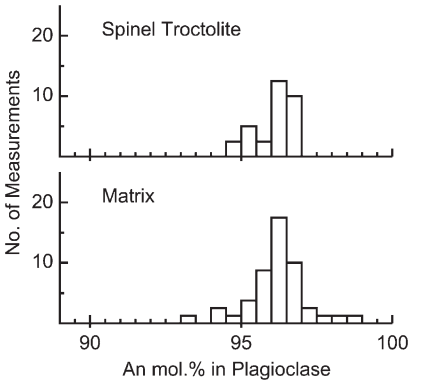

Fig. 4. Distribution of An values of plagioclase compositions in the spinel troctolite clast and fragments in the matrices of Dhofar 489.

PTS 11-3 (Table 1a) is 1.0×0.86 mm^2 in size. One grain of more ferroan olivine (Fo34) and only one zoned Fe–Ca-rich pyroxene grain ($Ca_{22}Mg_{36}Fe_{42}$–$Ca_{36}Mg_{28}Fe_{36}$–$Ca_{17}Mg_{27}Fe_{56}$) in the meteorite were found among five PTSs. Most of the pyroxene grains in the matrix have Mg numbers higher than 72 (Fig. 3); origin of the rare Fe–Ca-rich grain is not known.

The shapes of plagioclase fragments are not well defined in the dark matrices. Some large subrounded plagioclase grains in PTS 11-1 and 11-3 have dark rectangular cores with clear white rims. Many parts of the plagioclase clasts are converted to dark-colored, finely crystalline materials with small amounts of FeO and MgO. The second largest one, 1.8×0.6 mm^2 in size, shows twin lamellae. The An values of plagioclase in the PTS have much smaller range (An95–98) (Fig. 4) than those in other lunar anorthositic meteorites [6]. However, the peak is the same, i.e. An95–97. The An content of the acicular plagioclase in the crystalline matrix (An~96, Table 1b) is the same as that for large fragments.

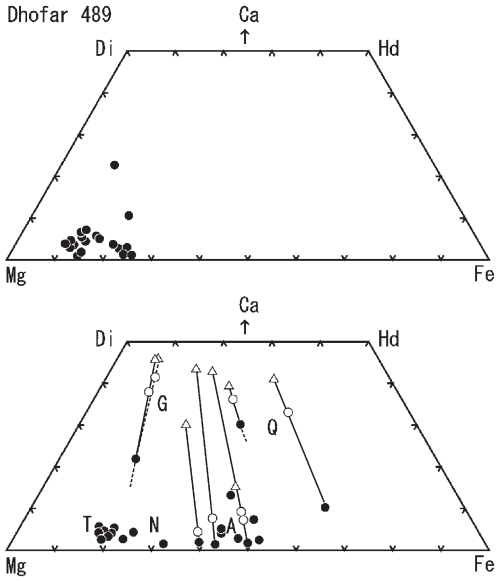

Fig. 3. Chemical compositions of pyroxene grains in the matrices of Dhofar 489 (top) and an Apollo anorthositic breccia 60016 (bottom). T: troctolite; N: norite; G: gabbro; A: anorthosite; Q: quartz monzodiorite.

Table 1b
Chemical compositions (wt.%) of plagioclases in Dhofar 489 lunar meteorite

	Spinel troctolite		Magnesian anorthosite		Large frag.[a]	Matrix	
			Oliv. gr[b]	Oliv. atch[c]	White rim	Acicular[d]	Bulk[e]
No.[f]	7	5	16	10	10	10	21
SiO_2	44.39	44.37	44.28	44.00	44.01	44.55	44.89
TiO_2	0.03	0.05	0.03	0.02	0.02	0.08	0.12
Al_2O_3	36.10	35.41	35.43	35.36	35.46	35.27	31.47
FeO	0.12	0.11	0.16	0.17	0.10	0.20	1.46
MnO	0.00	0	0.02	0.01	0.00	0.01	0.06
MgO	0.22	0.14	0.16	0.07	0.16	0.18	2.70
CaO	19.17	19.42	19.55	19.20	19.46	19.50	17.97
Na_2O	0.39	0.48	0.39	0.50	0.39	0.43	0.36
K_2O	0.03	0.02	0.01	0.02	0.01	0.01	0.01
Cr_2O_3	0.02	0.01	0.01	0.01	0.01	0.01	0.04
V_2O_3	0.01	0.01	0.01	0.01	0.00	0.00	0.00
NiO	0.01	0.01	0.02	0.01	0.03	0.00	0.00
P_2O_5	0.00	0	0.00	0.00	0.00	0.00	0.00
Total	100.51	100.04	100.06	99.48	99.65	100.25	99.14
Or	0.2	0.1	0.1	0.1	0.1	0.1	0.1
Ab	3.5	4.3	3.4	4.5	3.5	3.9	3.5
An	96.3	95.6	96.5	95.4	96.4	96.0	96.5

[a] Fragment.
[b] With granulitic olivines.
[c] With an olivine attached at a corner of the clast.
[d] Acicular plagioclase in crystalline matrix.
[e] Bulk matrix composition.
[f] Number of measurements.

Five anorthositic clasts with minor mafic silicates were recognized in PTS 2-1 and 11-3. They can be magnesian anorthosites or coarse-grained granulites. PTS 11 includes a large clast of spinel troctolite.

2.1. Magnesian anorthosite clasts

The second largest plagioclase-rich lithic clast (MA1, 3.0×1.3 mm^2 in size in PTS 2-1) contains an aggregate of amoeboidal mafic silicate (olivine) grains (0.7×0.4 mm^2; Fig. 1b). Although some mafic silicates show rounded grain shape, amounts and sizes of plagioclase are large and do not show granulitic texture. Because the twin lamellae of a plagioclase grain, one side attached to the olivine aggregate and the other terminated at the clast boundary, reach up to 1.6 mm, we conclude that this clast is a coarse-grained, crystalline anorthosite with twin texture, as was observed for 60025. Their olivine compositions (Fo79, Table 1a) are still more magnesian than those in the FAN trend. Thus, this clast could be a magnesian anorthosite.

2.2. Anorthosite clasts with mafic silicates

The largest angular fragment of plagioclase (MA2: 2.6×1.7 mm^2 in size) shows a shocked appearance, but the original rock could be an anorthosite. One brownish olivine crystal (0.42×0.14 mm^2) is attached at one edge of the clast. A determination of Fo75 indicates that this clast is also magnesian anorthosite. Some subrounded plagioclases (e.g. AN2) in PTS 11-3 have fine-grained, rectangular, dusty inclusions with a clear rim. One such clast (AN1) contains a very small olivine with Mg number 78.

2.3. Coarse-grained granulite-like clast

One clast (GR1) in PTS 2-1, 1.0×0.7 mm^2 in size has a chain of mafic silicates 1.0×0.13 mm^2. Rounded shapes of the olivine grains suggest that this may be a coarse-grained granulite. Another shocked plagioclase-rich clast (GR2: 2.2×1.5 mm^2 in size in PTS 11-3) includes more than 15 rounded olivine grains less than 0.1 mm in diameter. This clast may be a granulite, but we cannot see the detailed textures because of the shock effects.

2.4. Spinel troctolite clast

PTS 11 includes a crystalline clast 4.1×1.3 mm^2 in size and containing coarse crystals of mafic silicates [12]. The lithic texture of this clast, showing elongated, oval-shaped, olivine crystals (Fig. 1d), resembles those of some spinel troctolite clasts (e.g., 67435) [13]. However, olivine crystals in this clast have more rounded euhedral forms, perhaps because of metamorphism. Minor pyroxene grains (Table 1a) in the clast are found at the junction of few large olivine grains and as isolated crystals. High-Ca pyroxene crystals ($Ca_{50}Mg_{44}Fe_6$) occur in contact with low-Ca pyroxene crystals ($Ca_3Mg_{83}Fe_{14}$) or as isolated crystals. The plagioclase matrix is recrystallized and fine-grained. Rounded, brownish spinel grains are included in both plagioclase and olivine. The Fo contents of olivine (Fo84) represent one peak of the bimodal distribution described above. The An values of plagioclase (An96; Fig. 4) in the clast are in the middle of the distribution (An95–98) of plagioclase fragments in the matrix [12].

The Cr/(Cr+Al) atomic ratio of the spinel grains enclosed in plagioclase is 0.30 and the Fe/(Fe+Mg) ratio is 0.35. The Cr ratio of spinel grains enclosed in olivine is 0.7, and the Fe ratio is 0.6. A few spinel grains with similar composition were found in one small clast in PTS 1. The spinel compositions of Dhofar 489 (Table 1a) are similar to, but slightly more Cr-rich, than those of chromian spinels (pleonastes) in the Apollo spinel troctolites (e.g., 67435, 72435, 73263) [13,14].

The modal abundances (in area %) of the minerals of the spinel troctolite are: plagioclase 72, olivine 25, orthopyroxene 2.2, augite 0.5, and spinel 0.3. The

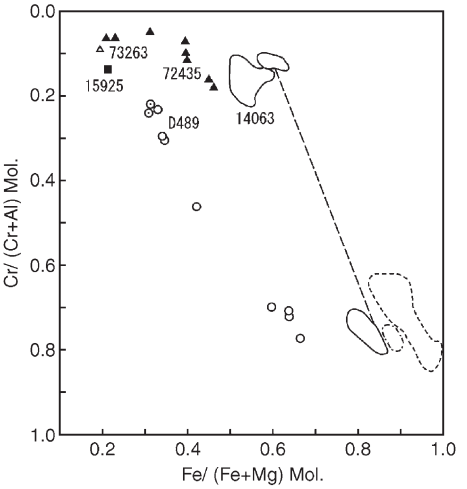

Fig. 5. The spinel compositions of the spinel troctolite (ST) clast in Dhofar 489 (open circles) plotted in a base projection of the multicomponent spinel prism. The Cr/(Cr+Al) atomic ratios vs. Fe/(Fe+Mg) ratios of the spinels in Dhofar 489 are compared with those of Apollo spinel troctolites (15925, 72435, 73263) and spinels in the Apollo 14 breccias (14063). Open circle with a dot is a spinel in the small ST clast of Dhofar 489.

mineral assemblage of the Dhofar 489 clast is similar to that of spinel troctolite 67435,14 [13,15]. The mafic silicates in the Dhofar 489 clast have a granulitic texture, but the grain size of the olivine is much coarser (from 0.15×0.08 up to 0.69×0.23 mm^2 in size) than common granulites. The Dhofar 489 spinel compositions plotted in a base projection of the multicomponent spinel prism (Fig. 5) shown in Haggerty [14] are within the same region as the Apollo spinel troctolites. A consideration of the system diopside–forsterite–anorthite for the parent magma of these rocks indicates that certain liquids would crystallize spinel as one of the earliest phases [15]. Based on the stability relations of the cordierite-to-spinel–cataclasite (shocked spinel troctolite) transition, Herzberg and Baker [15] showed that spinel cataclasites from Apollo 15 and 17 were located at depths of greater than or equal to about 12 to 32 km prior to excavation. The Dhofar spinel troctolite may have a similar origin.

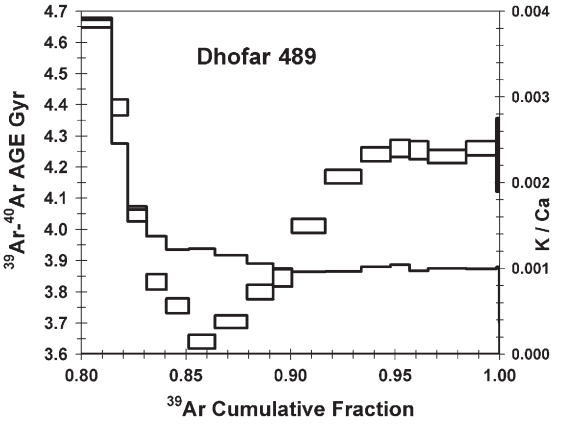

Fig. 6. ^{39}Ar–^{40}Ar age (rectangles, left scale) and K/Ca ratios (stepped line, right scale) for stepwise temperature extractions of Dhofar 489 whole rock for temperatures >700 °C. This portion of the age spectrum represents ~108 ppm K. Because the first ~80% of the ^{39}Ar release is dominated by terrestrial contamination, only data for the last 20% of the ^{39}Ar release are shown.

3. ^{39}Ar–^{40}Ar age determination

At NASA–JSC, a whole rock chip of a feldspathic clast in Dhofar 489 was broken into several smaller pieces, which were treated for 5 min. with 2 N HNO_3 to remove some of the terrestrial weathering product obviously present. A 63.6 mg sample was packaged with other samples and irradiated with fast neutrons at the University of Missouri Research Reactor. Multiple samples of standard hornblende NL25 in this irradiation defined an irradiation constant (J-value) of 0.02685 ± 0.00010. Argon was extracted from Dhofar 489 by stepwise temperature release and its isotopic composition was measured on a mass spectrometer. Corrections were made for instrument mass discrimination, system blanks, radioactive decay, and reactor interferences. The Ar–Ar age was calculated from the corrected ^{40}Ar/^{39}Ar ratio by comparison to this ratio measured in the hornblende [16]. Uncertainties in individual ages were calculated from uncertainties in the measured ^{39}Ar/^{40}Ar ratios and in corrections for blanks and reactor interferences.

A portion of the Dhofar 489 Ar–Ar age spectrum that released 80% to 100% of the total ^{39}Ar (670–1425 °C extractions) is shown in Fig. 6. The first (400 °C) extraction (not shown in Fig. 6) released 75% of the total ^{39}Ar, equivalent to 400 ppm K with a K/Ca ratio of 0.04. The apparent Ar–Ar age of this extraction was only 0.14 Gyr. We attribute essentially all of this K to terrestrial weathering products on grain surfaces. Hot desert meteorites commonly contain such phases. The second and third extractions (500 and 600 °C, not shown in Fig. 6) released 4.3% of the total ^{39}Ar, showed elevated ^{36}Ar/^{37}Ar ratios, and gave apparent Ar ages of 6.0–6.3 Gyr. We attribute these high ages to terrestrial atmospheric ^{40}Ar adsorbed on weathered grain surfaces. In support of this conclusion is the observation that an isochron plot (R^2 = 0.998) of ^{40}Ar/^{36}Ar vs. ^{39}Ar/^{36}Ar for the second through fifth extractions releasing 75% to 82% of the ^{39}Ar gives a negative slope, indicating release of ^{39}Ar unaccompanied by radiogenic ^{40}Ar, and a ^{40}Ar/^{36}Ar intercept close to the terrestrial atmospheric value.

For those extractions releasing ~80% to 85% of the ^{39}Ar (Fig. 6) the age declines down to a value of 3.65 Gyr and the K/Ca ratio continues to decrease, as Ar release from weathering product is exhausted. Above ~84% of the ^{39}Ar release the K/Ca ratio is essentially constant at ~0.001 and probably represents that portion of these elements indigeneous to the sample, uncontaminated by terrestrial weathering. We estimate the indigenous concentrations of K and Ca in our Dhofar 489 sample to be ~90 ppm and ~11%, respectively, values typical of unweathered lunar feldspathic rocks. Over ~85% to 93% of the ^{39}Ar release the Ar age increases in a manner suggesting prior loss of some radiogenic ^{40}Ar by diffusion. Six extractions (1200–1340 °C), releasing the last ~7% of the total ^{39}Ar, define a plateau in Ar age with a mean value of 4.246 ± 0.013 Gyr (1σ). An isochron plot of ^{40}Ar/^{36}Ar vs. ^{39}Ar/^{36}Ar (R^2 = 0.9987, using measured ^{36}Ar) for the six extractions that define the age plateau yields a similar Ar–Ar age of 4.247 ± 0.030 Gyr and a ^{40}Ar/^{36}Ar intercept of −0.93 ± 3.0 (2σ). The fact that in situ radiogenic ^{40}Ar in lunar anorthosite degasses at much higher temperature than does Ar in weathering products permitted, in this sample, the

complete resolution of indigenous ^{40}Ar against a much larger background of terrestrial Ar.

In most materials the uncertainty in the Ar–Ar age derives from uncertainties in the measured $^{40}Ar/^{39}Ar$ ratio and in the irradiation constant determined from the standard age monitor. However, for lunar materials with low K/Ca ratios, two additional factors can contribute significantly to the uncertainty in the age. These factors are the magnitude of a correction applied for ^{39}Ar produced in the reactor from Ca and of a correction that may be required for lunar atmosphere ^{40}Ar incorporated into the sample along with solar wind ^{36}Ar. Much of the reported uncertainty in the Ar–Ar age for Dhofar 489 derives from the ~29% correction applied for ^{39}Ar produced in the reactor from Ca. The magnitude and uncertainty of this reactor correction was determined by measuring the $^{39}Ar/^{37}Ar$ ratio in multiple samples of pure CaF_2 irradiated at different times in the same reactor position.

We considered corrections to the age for trapped ^{40}Ar as follows. Concentrations of ^{36}Ar and ^{38}Ar in Dhofar 489 may derive from several sources: cosmogenic Ar produced from Ca; ^{38}Ar produced during neutron irradiation from Cl in the sample; and possible solar wind Ar acquired on the moon. Argon-37 is produced from Ca in the reactor and is expected to strongly correlate with cosmogenic Ar. We refer to cosmogenic Ar plus ^{37}Ar as a nuclear component. To apply a possible correction to the Dhofar 489 age for lunar atmosphere ^{40}Ar, we need to know the amount of trapped solar wind ^{36}Ar present (if any) and the trapped lunar $^{40}Ar/^{36}Ar$ ratio. We examine only those extractions releasing >85% of the total ^{39}Ar (Fig. 6). The maximum amount of cosmogenic $^{36}Ar_{cos}$ released in these extractions can be estimated from the minimum measured $^{36}Ar/^{37}Ar$ ratio of 0.0030 observed at a temperature of 1315 °C [17]. Because total ^{36}Ar equals cosmogenic ^{36}Ar plus solar ^{36}Ar, this calculation also defines the minimum amount of solar wind ^{36}Ar released in the other extractions.

To estimate the minimum amount of $^{36}Ar_{cos}$ and thus the maximum amount of (trapped) $^{36}Ar_{tp}$, we now consider ^{38}Ar. The observation that measured $^{36}Ar/^{38}Ar$ ratios are lower than the expected trapped ratio of ~5.3 and that most are lower than the expected cosmogenic ratio of 0.67 indicates that most of the ^{38}Ar was made in the reactor from ^{37}Cl [17]. Further, because the abundance of $^{36}Ar_{cos}$ exceeds that of $^{36}Ar_{tp}$, the abundance of $^{38}Ar_{cos}$ should significantly exceed the abundance of $^{38}Ar_{tp}$. Thus, to a first approximation a plot of $^{36}Ar/^{38}Ar$ vs. $^{36}Ar/^{37}Ar$ for the last 14% of the ^{39}Ar release (Fig. 7) shows the relationship of a mixture of

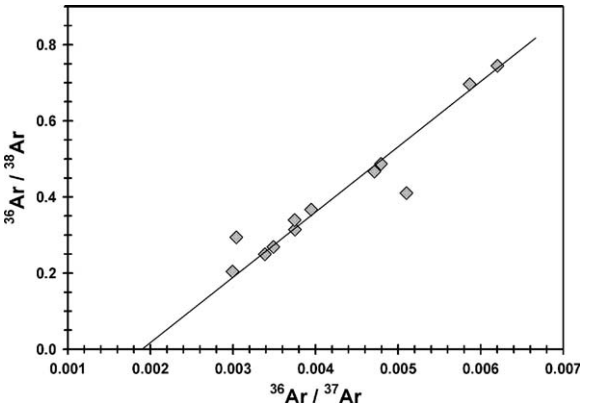

Fig. 7. Plot of $^{36}Ar/^{38}Ar$ vs. $^{36}Ar/^{37}Ar$ ratios of Dhofar 489 for the 1000–1340 °C extractions releasing >85% of the total ^{39}Ar.

three components – a $^{36}Ar+^{37}Ar+^{38}Ar$ nuclear component, $^{36}Ar_{tp}$, and large amounts of (Cl-derived) $^{38}Ar_{Cl}$. The $^{36}Ar/^{37}Ar$ ratio decreases to the lower left as $^{36}Ar_{tp}$ decreases relative to $^{36}Ar_{cos}$, and the $^{36}Ar/^{38}Ar$ ratio decreases as $^{38}Ar_{Cl}$ increases relative to $^{38}Ar_{cos}$. With three components present, data in Fig. 7 could, in principle, show random scatter. Instead, the linear trend in Fig. 7 implies that release of $^{38}Ar_{cl}$ is correlated with release of $^{38}Ar_{cos}$. This might result if terrestrial Cl contamination were introduced into the meteorite as $CaCl_2$, although this does not explain the relatively high temperature release of the $^{38}Ar_{Cl}$. We utilize the strong linear trend shown by 10 of 12 plotted data ($R^2=0.997$) to define $^{36}Ar/^{37}Ar=0.0019$ at $^{36}Ar/^{38}Ar=0$. We adopt this intercept as a minimum value for $^{36}Ar_{cos}$ and thus a maximum value for $^{36}Ar_{tp}$, because $^{36}Ar/^{38}Ar$ ratios less than zero are not permitted. This consideration yields a maximum concentration of solar ^{36}Ar that is a factor of 1.9 larger than that obtained above from consideration of the minimum observed $^{36}Ar/^{37}Ar$ ratio. Because $^{36}Ar/^{38}Ar=0$ in Fig. 7 would imply that all ^{38}Ar were produced from Cl and no cosmogenic ^{38}Ar is present, we consider the maximum correction for solar ^{36}Ar to be too large.

The trapped $^{40}Ar/^{36}Ar$ ratio in our Dhofar 489 clast is not known. However, the isochron intercept of $^{40}Ar/^{36}Ar=-0.93\pm3.0$ may suggest that this ratio is not greater than ~2. Most lunar regolith materials show trapped $^{40}Ar/^{36}Ar$ ratios ranging from ~0.5 up to ~9 for a few very old breccias [18]. Thus, we applied a correction for lunar atmosphere ^{40}Ar based on assumed ratios for $^{40}Ar/^{36}Ar$ of 2 and 9, and based on the upper and lower limits of solar ^{36}Ar concentrations obtained above. Applied corrections based on trapped $^{40}Ar/^{36}Ar=2$ produce corrected Ar–Ar ages of 4.241–4.233 Gyr, compared to the uncorrected age of 4.246±0.013 Gyr.

Corrections based on $^{40}Ar/^{36}Ar=9$, using the upper and lower limits to the cosmogenic $^{36}Ar/^{37}Ar$ ratio, produce ages of 4.222 to 4.189 Gyr. We conclude that the Ar–Ar degassing age of our Dhofar 489 clast lies between 4.18 and 4.25 Gyr, with a most probable value nearer the upper limit, i.e., 4.23±0.03 Gyr.

4. Major and trace element chemistry and the farside origin

Two chips were separated from different portions of the 6.83 g Dhofar 489 slab at NSMT for the determination of bulk major and trace element chemistry. These chips, named specimens c and d, weighed 143 and 31 mg, respectively. Chip d2 is a subsplit of a white anorthositic clast from the d sample and d1 is a remainder. Specimens c and d1 are representative bulk samples. Major element concentrations were determined by prompt gamma-ray analysis (PGA) [19]. Before assaying to PGA, two chips were pulverized in an agate mortar. Whole samples were shielded inside FEP bags and analyzed by PGA using a thermal neutron beam guided out of the JRR-3M reactor at the Japan Atomic Energy Research Institute (JAERI). Most major and minor elements were determined by PGA. After PGA, some portions (about 10 mg each) of the specimens once used for PGA were reused for the determination of rare earth elements (REEs), Th and U. These elements were determined by inductively coupled plasma mass spectrometry (ICP–MS) at Tokyo Metropolitan Univ. (Hayano and Ebihara, 2005, personal communication). Both PGA and ICP–MS data are summarized in Table 2 and are compared with those of Dhofar 025, Y 791197 [7], and Apollo 16 highland sample, 67513 [20]. Errors

Table 2
Elemental abundances of Dhofar 489 and related lunar meteorites

	Dhofar 489						67513 [b] (I)	Dhofar 025 [c] (II)	Y 791197 [c] (III)
	c (bulk)	Error [a]	d1 (bulk)	Error [a]	d2 (An)	Error [a]			
SiO_2 (%)	43.5	0.9	43.9	1.4	42.5	1.2	45.2	44.2	44.9
TiO_2 (%)	0.104	0.007	0.120	0.014			0.37	0.290	0.40
Al_2O_3 (%)	27.7	0.4	29.8	0.6	31.7	0.5	27.8	26.9	27.3
Cr_2O_3 (%)	0.0644	0.0003	0.0564	0.0004	0.0080	0.0001	0.11	0.11	0.11
FeO (%)	3.28	0.02	2.83	0.03	0.46	0.01	5.63	4.90	5.71
MnO (%)	0.0473	0.0019	0.0376	0.0026	0.0114	0.0012	0.11	0.05	0.12
MgO (%)	6.51	0.47	5.58	0.68	2.37	0.30	4.02	7.10	5.76
CaO (%)	15.7	1.0	17.2	0.4	18.5	1.4	16.7	16.20	15.86
Na_2O (%)	0.371	0.001	0.360	0.001	0.480	0.001	0.31	0.35	0.30
K_2O (%)	0.0361	0.0119	0.0709	0.0253			0.016	0.039	0.028
P_2O_5 (%)							0.02	0.06	0.02
Total (%)	97.3	1.5	100.0	1.7	96.1	1.9	100.3	100.2	100.5
La (ppm)	0.727	0.023	0.645	0.012	0.405	0.010	1.34	3.27	1.93
Ce (ppm)	1.56	0.03	1.31	0.02	0.545	0.010	3.84	8.71	5.18
Pr (ppm)	0.251	0.006	0.224	0.006	0.116	0.004			
Nd (ppm)	0.986	0.029	0.831	0.023	0.333	0.016		5.1	3.0
Sm (ppm)	0.291	0.009	0.241	0.013	0.072	0.010	0.781	1.646	0.975
Eu (ppm)	0.718	0.019	0.668	0.011	0.802	0.015	0.752	0.819	0.734
Gd (ppm)	0.353	0.010	0.300	0.020	0.117	0.010			
Tb (ppm)	0.0613	0.0027	0.0525	0.0031	0.0126	0.0008	0.194	0.337	0.227
Dy (ppm)	0.400	0.017	0.351	0.012	0.074	0.003			
Ho (ppm)	0.0857	0.0049	0.0781	0.0027	0.0184	0.0011			
Er (ppm)	0.254	0.010	0.225	0.012	0.046	0.002			
Tm (ppm)	0.0371	0.0015	0.0327	0.0016	0.0057	0.0005			
Yb (ppm)	0.241	0.012	0.214	0.003	0.045	0.003	0.834	1.280	0.896
Lu (ppm)	0.0360	0.0007	0.0315	0.0022	0.0046	0.0004	0.124	0.179	0.127
Th (ppm)	0.0634	0.0021	0.0551	0.0030	0.0118	0.0009	0.142	0.525	0.291
U (ppm)	0.156	0.004	0.143	0.006	0.241	0.011	<0.2	0.20	0.09
Sum REE (ppm)	6.00		5.20		2.61		7.87	21.34	13.07
Mg/(Fe+Mg) (mol)	0.780		0.778		0.901		0.560	0.721	0.643

[a] Errors are due to counting statistics (1σ) in γ-ray counting for elements except for REE, Th and U, for which values of standard deviations ($n=5$) in ICP–MS are quoted.
[b] Jolliff and Haskin [20].
[c] Korotev et al. [7].

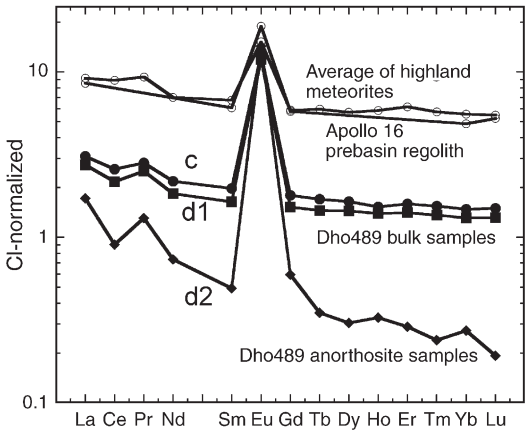

Fig. 8. CI-chondrite normalized REE patterns for bulk samples (c and d1) and anorthositic clast d2 of Dhofar 489(Dho489), lunar highland meteorites and the Apollo 16 regolith.

quoted for major and minor elements (expressed as oxides) are due to counting statistics (1σ) in PGA, while those for REEs, Th and U represent standard deviations (1σ) of three successive measurements in ICP–MS. Chemical compositions of specimens c and d1 (Table 2) are similar to each other, except for a few elements such as Mn and especially K. In fact, except for K, major and minor elemental contents of both specimens are identical with a ratio of 1.05 ± 0.14 (1σ), suggesting that these values represent the bulk composition of the meteorite. Inconsistencies noticed in K and Mn data between the two specimens may be terrestrial weathering.

REE abundances, however, show a systematic difference between the two specimens, with specimen c having 15% higher abundances than those of specimen d1. It is remarkable that the difference is consistent among REEs, as suggested by a small value of the relative standard deviation (3.4%). CI-normalized REE abundance patterns of Dhofar 489 are illustrated in Fig. 8, and are compared with patterns for an average of highland meteorites and Apollo 16 pre-basin regolith. Th and U data also show systematic difference between the two samples. The lowest REE abundance, in split d2, is consistent with the white anorthositic appearance. The high CaO content of split d2 also support high anorthite content. The REE abundance of Dhofar 489 is much lower than those for other samples shown in Fig. 8. In fact, the Dhofar 489 REE abundance is the lowest among lunar feldspathic meteorites [7]. The Th content of Dhofar 489 is also lower than those of any other lunar samples or lunar feldspathic meteorites. However, in Dhofar 489, U values are anomalously high, with Th/U ratio being about 0.4, which is 10 times lower than other feldspathic meteorites. The high abundance of U must be explained in terms of terrestrial weathering in the hot desert, which may also explain the higher abundance of Ca in split d1 than other feldspathic meteorites. In our analytical procedure, acid chemical leaching for selective dissolution of terrestrial contaminants, like Ca carbonate, was not applied, because acid leaching may also dissolve Ca-phosphate (whitlockite and apatite), which is a major carrier for REE, Th and U [21].

Concentrations of REE and Th for the two Dhofar bulk samples, c and d1 (Table 2) are among the lowest for lunar feldspathic meteorites [7]. FeO contents of Dhofar 489 also are lower than those of common lunar feldspathic rocks. The low bulk FeO concentration is consistent with the occurrence of anorthositic clasts with very low abundance of mafic silicates of high Mg number. Fig. 9 shows a correlation between Th (ppm) and FeO (wt.%) for lunar feldspathic materials, including the Dhofar 489 meteorite. Dhofar 489 plots at the lowest concentrations among these materials. Low concentrations of the incompatible elements such as REE, Th, and U in Dhofar 489 strongly suggest that this meteorite was derived a large distance away from the PKT [3].

Siderophile element data may give us a hint for discussing the genesis of Dhofar 489, or at least the Dhofar 489 magnesian anorthosites. We obtained only preliminary data of two siderophile elements, Ni and Co by INAA and found Ni/Co mass ratios to be about 5–6 for bulk samples (c and d1), demonstrating that they are not mixtures of unrelated felsic and mafic components [22]. Although Ni in the anorthosite-rich sample (d2) is below detection limit, the low bulk Ni/Co ratio suggests that the major rock type of this meteorite may have a

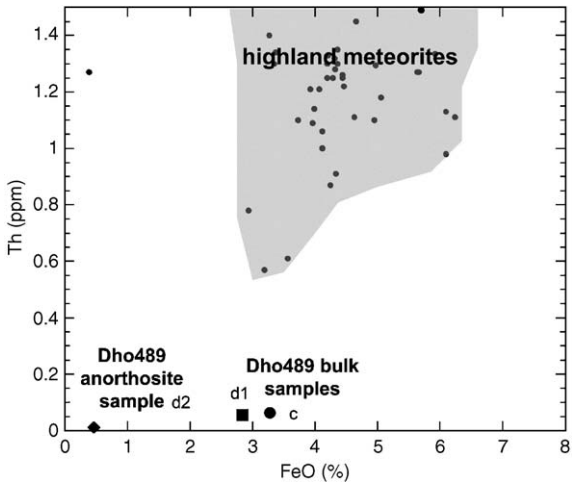

Fig. 9. Th (ppm) vs. FeO (wt.%) diagram for bulk samples (c and d1) and anorthositic clast d2 of Dhofar 489(Dho489) and related samples.

similar ratio. Thus, an igneous origin of the Dhofar 489 magnesian anorthosites is not difficult to propose, because such rock type is the major component of this meteorite. Metallic phases were not detected in the magnesian anorthosite clast, but a low abundance of metal with low Ni/Co of the bulk sample would be consistent with an igneous origin of the major components of the meteorite.

In addition, Ti/Sm ratios of the two splits of Dhofar 489 (2100 and 3000 for c and d1, respectively; mass ratios) (Table 2) are well within the range of nearside ferroan anorthosites [22], and clearly distinct from the much lower Ti/Sm of nearside Mg-suite rocks. The near-chondritic Ti/Sm of Dhofar 489 indicates a lack of KREEP contamination, and may indicate affinities with anorthosites. Ti/Sm ratios of Dhofar 489 distribute along the magnesian extension of the FAN region in the Ti/Sm vs. Mg number diagram of Cohen et al. [23], and not along the extension of the lunar feldspathic meteorites and granulitic breccias, which distribute mostly below the FAN region.

Warren [24] reported implications of new data on lunar meteorites for composition of the global lunar surface, lunar crust, and the bulk Moon. Among the lunar meteorites, his two Th-poor samples (0.20 μg/g Th) are still higher than that of Dhofar 489 reported in this paper. If Dhofar 489 is a representative rock of the farside highland, our conclusion is consistent with the statement by Warren that an important component of the Moon is highly magnesian.

5. Differentiation trends of the anorthositic crust

Granulitic breccias and granulites are coherent crystalline rocks that have been recrystallized by heating at temperatures over 1000 °C for long periods of time [25]. The textures are characterized by rounded polyhedral grain shapes or the presence of many small grains within fewer larger grains [9]. Granulitic breccias contain relicts of clasts, whereas granulites do not. Both commonly consist of a mosaic of grains whose boundaries meet at angles of about 120°, a texture produced by thorough recrystallization. “Lunar granulites” have an astonishing diversity of textures ranging from fine-grained, barely annealed hornfels, to coarse-grained rocks with well-equilibrated textures, to rocks with relict melt textures (see Cushing et al. [26]).

Many granulitic clasts found in the Apollo highland breccias [9] and many lunar meteorites (e.g., [6,7,9,10]) have plagioclase An values and coexisting mafic mineral Mg number that plot within the “gap” separating ferroan anorthosite suite (FAN) and high magnesium

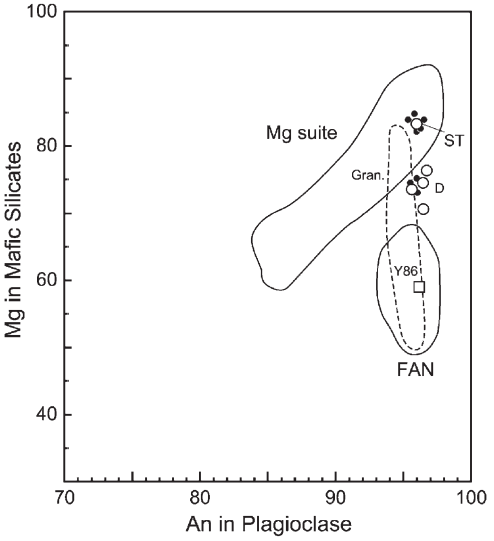

Fig. 10. Chemical compositions of magnesian anorthosites (large open circles, D) and a spinel troctolite (ST) in Dhofar 489 plotted in the plagioclase An values [Ca/(Ca+Na+K) mol%] vs. coexisting mafic mineral Mg numbers diagram of the Apollo samples. Two classical differentiation trends are ferroan anorthosite suite (FAN) and high Mg suite (HMS) rocks. These patterns are compared to granulitic trend (Gran.) in Antarctic lunar meteorites and a FAN clast in Y86032 (Y86). Small solid circles are mineral pairs (explanation in the text) in the crystalline part without clear clast–matrix boundaries of Dhofar 489.

suite (HMS) rocks (Fig. 10). Such granulites are more abundant than FANs in some lunar meteorites [6,11]. Dhofar 025 described by Cahill et al. [6], for example, contains magnesian granulites, as well as FAN components. There have been a number of previous proposals that mineral compositions falling into the “gap” represent igneous compositions, but this idea has met widespread resistance because such rocks can always be shown to represent mixed lithologies, generally referred to as granulitic breccias, rather than true igneous rocks [27]. Some granulitic clasts plotting within the “gap” lost their breccia textures [9] by thermal metamorphism from the heat of large impacts, such that solid state recrystallization has occurred [28]. Magnesian granulitic breccias clearly are derived from high-Mg number, olivine-bearing, but plagioclase-rich lithology of the feldspathic crust. However, no crystalline precursor rock has been recognized in the lunar samples. The Mg number of the spinel troctolite in Dhofar 489 plots at the top of the HMS trend in Fig. 10 and is more magnesian than the common magnesian granulites.

Although the mafic silicates we found in the magnesian anorthositic clast (MA1) in Dhofar 489 show a subrounded texture, the over all textures do not have remnants of a breccia texture and are different from those of the lunar granulitic breccias as given above

[25,26]. The amounts of plagioclase are larger than those for most granulites. The presence of twin lamellae extending to a large part of the clast (Fig. 1 in Takeda et al. [29]) indicates that this clast is not a granulite. Such twin textures were observed for ferroan anorthosites such as 60025. Such twin lamellae texture will not be preserved if shock produced twin textures were annealed by a subsequent metamorphic event to produce granulites. Any grains of olivine in a rock formed very early in the history of the primary lunar crust may show subrounded outer shapes produced by the heat of the hot crust. The rounded olivine crystals in pallasites are a good example of such materials [30]. MA2, MA1 and AN2 clasts do not have granulitic textures as given above. We suggest that three magnesian anorthositic clasts in Dhofar 489 represent a major rock-type of the farside of the Moon. The Ni/Co and Ti/Sm data discussed above also support the igneous origin of these anorthositic clasts.

The magnesian anorthosite clasts in Dhofar 489 with the lowest Mg contents (An96.5, Fo71.6) define a Mg-rich extension of the FAN trend in the An vs. Mg number diagram in Fig. 10. Such a magnesian trend as found in the Dhofar 489 anorthositic clasts was reported for the Stillwater layered intrusion [31]. Therefore, the starting point for the crystallization of mafic silicates in the earliest crust of the farside of the Moon could be more magnesian than the Apollo FAN trend. This magnesian trend may imply a trend more primitive than the FAN trend.

Four anorthositic lithic clasts were recognized in one PTS (2-1), but the most ferroan olivine in this clast is still more magnesian than those in the FAN trend. The Fo contents of these clasts represent the Fo-poor peak of the bimodal Fo distribution in Fig. 2. Their Mg numbers and the An values plot in the gap in Fig. 10. The pair indicated as "mineral pair" in Fig. 10 represents a composition of the mafic silicate surrounded by plagioclases in crystalline contact, but their clast boundaries could not be recognized due to shock disturbances. The trends of the mineral pairs are the same as that of the clasts. If we assume that other mineral grains of the Fo-poor peak in Fig. 2 are from unknown dunites, troctolite or norite materials, we have to propose the presence of "pure" anorthosites to mix with such mafic silicates. The Ni/Co and Sm/Ti data of Dhofar 489 also exclude the mixtures of the Mg-suite rocks. It is more reasonable to accept the idea that magnesian anorthosites exist.

Papike et al. [25] described some mineral pairs, which extend the region of the HMS towards the Mg-poor side in Fig. 10, and which cause the FAN trend to expand slightly more in the magnesian direction. However, the pristinity of these rocks are not well documented, and they are from the PKT. Finally, the magnesian granulites have been argued by Korotev to be a special product of the PKT [32]. Our proposal, that Dhofar 489 is mixtures of magnesian anorthosites with spinel troctolites from the lunar farside, would not argue against Korotev's interpretation, because low-Th of Dhofar 489 indicates that it is not from the PKT. The old Ar–Ar age and remote sensing data suggest that the petrologic formation of these rocks is older and more widespread on the farside.

6. Rocks from the lunar farside

Several "pristine" lunar highland rocks, such as ferroan–anorthosites, Mg-suite rocks, and alkali-suite rocks, give ages by various radiometric techniques in the range of 4.0–4.5 Gyr [33]. Some of these old ages probably date the original formation time of these rocks. In contrast, a significant number of additional lunar highland samples give younger radiometric ages of ~3.8–4.0 Gyr that have been reset by impact heating [34,35]. The K–Ar chronometer is the most easily reset by impact, and almost all Ar–Ar ages of highland rocks probably reflect the time of post-formation impact heating [36]. Turner [37] gave an extensive summary of Ar–Ar ages of lunar highland rocks, including many anorthosites and other feldspathic samples. The oldest Ar–Ar age among these feldspathic samples is ~4.2 Gyr (updated to new ^{40}K decay constants). An open question about the early lunar impact history is whether major impacts occurred across the broad time period of ~4.5–3.8 Gyr ago [38], or were concentrated in a cataclysmic period ~4.0–3.8 Gyr ago [39]. The concentration of Ar–Ar ages of lunar highland rocks below 4.0 Gyr might indicate the second impact model. However, most of these dated samples returned by Apollo were collected across a limited area of the lunar surface that was strongly influenced by the Imbrium and Serenitatis impacts, both of which occurred <3.9 Gyr ago [39]. Thus, the value of measuring Ar–Ar ages of anorthositic clasts in meteorite highland breccias such as Dhofar 489 lies in the high probability that most such meteorites derived from portions of the Moon far remote from the large, young impact basins sampled by Apollo.

The Dhofar 489 Ar–Ar age of 4.23±0.03 Gyr ranks among the very oldest Ar–Ar ages for lunar highland feldspathic rocks (e.g., [40]). The age of Dhofar 489 is younger than the Ar–Ar age of 4.35–4.40 Gyr previously reported for an anorthositic clast in another lunar meteorite, Yamato 86032 [40], which belongs to the

FAN family [41]. The Ar–Ar age of Dhofar 489 may represent the formation time of the crystalline matrix, likely involving a large impact and metamorphism of the entire breccia. Although the older Ar–Ar ages for the Dhofar 489 and Y86032 meteorites are only two examples, they are consistent with some degree of continual lunar bombardment in the period 4.4–4.1 Gyr ago, absent a sufficiently high impact rate so as to destroy all surface rocks as proposed by Hartmann [38].

Bussey and Spudis [42] used full-resolution Clementine images to perform compositional studies of four large lunar basins. They reported that inner rings of all four basins display massifs of nearly "pure" anorthosite (FeO < 1 wt.%), virtually the only known occurrences of this rock type on the Moon. Hawke et al. [43] also reported distribution and modes of occurrence of lunar anorthosites, in support of the discussion of anorthosite exposures in the rings of lunar basins. The presence of one small mafic silicate grain with Mg number 78 in the largest white anorthositic clast (PTS 11-3, AN2) suggests that "pure" anorthosites of Bussey and Spudis [42] may also be a magnesian anorthosite with very low abundance of mafic silicates of high Mg number.

Presence of a magnesian anorthositic rock type in the lunar highland was also proposed by Lucey and Cahill [44], based on remote-sensing data from Lunar Prospector and Clementine. They found that while there is overlap in occurrences, the ferroan compositions are mainly concentrated on the nearside and the lunar south, and magnesian compositions occur more frequently on the farside and the lunar north. Although a real relation between Dhofar 489 and the magnesian compositions proposed by [44] is not known, these observations support the inference from the Dhofar 489 lunar meteorite that magnesian feldspathic material can be widespread, but occurs mainly distant from the Apollo zone.

Korotev [45] also reported briefly the geochemistry of some Dhofar lunar meteorites, excluding the trace element data of Dhofar 489, and recognized that these crystalline impact melt breccias are dominated by magnesian anorthosite. His magnesian anorthosite is a breccia composed in large part of some type of magnesian anorthosite that is not well represented by samples in the Apollo collection. However, he did not give any mineralogical and petrographical characteristics of the magnesian anorthosite. We suggest that the magnesian anorthosite clasts found in Dhofar 489 are what he called magnesian anorthosite.

Using Lunar Prospector gamma-ray data, Lawrence et al. [46] observed a Mg-rich region northwest of Crisium. The FeO-poor material could be a spinel troctolite, excavated from depth by this basin. This spinel troctolite is different from locally derived ones at the PKT. If, as proposed by Bussey and Spudis [42], nearly "pure" anorthosites were mixed with any other rocks with magnesian mafic silicates, magnesian granulitic breccias common in the lunar highlands could be produced. However, the second component can be magnesian anorthosites similar to Dhofar 489. Two distinct peaks in the bimodal Fo distribution of the entire meteorite (Fig. 2) suggest that they represent two unique lithologies of the farside crust. The Fo-poor one could be the magnesian anorthosite clasts found in Dhofar 489 PTS 2-1. The range of the Fo distribution of each peak of Fig. 2 suggests that these olivine grains were not homogenized after breccia formation by diffusion of Fe/Mg.

Although a combination of these proposals can explain the origin of low-FeO anorthositic breccias, the location of four large basins (above) close to the PKT would not define the specific origin for the Dhofar 489 meteorite. Because the farside highlands above the equator have low-Th, and a high-Mg number [1–3], a possible source basin for Dhofar 489 on the farside is more likely. In addition, the presence of magnesian anorthosites extending into the "gap" of the An vs. Mg number diagram cannot be excluded as characteristic of an early formed lunar crust for the farside highlands.

Lindstrom et al. [47] reported magnesian anorthosites associated with troctolites in an Apollo 14 breccia. They suggested that these rocks are distributed in a regional rather than a global manner. Dhofar 489 differs from such local products, because the spinel troctolites are believed to be excavated from the deep-seated crust [15]. The trace element data indicate that the Dhofar 489 spinel troctolite is not from the PKT. Because one of two frequent compositions of magnesian olivine grains in the matrix of Dhofar 489 is the same as those in the spinel troctolite clast, it is possible to think that the Dhofar 489 breccia can be mixtures of magnesian anorthosites and spinel troctolite without major FAN-like components. The spinel troctolite clast (Fig. 1d) we found is located at the top of the HMS trend in Fig. 10, and is the most plausible example of the early formed, deeper lunar crust of the farside.

7. Conclusions

We present new petrologic descriptions, major and trace element data, and Ar–Ar age data on lunar meteorite Dhofar 489. The significance of this particular lunar meteorite is that it has the lowest concentrations of incompatible trace elements of any lunar meteorite. It plausibly provides a unique sample of large areas of the

farside crust of the Moon, which have been mapped from orbit but not explored by the Apollo missions. Because of the low Th, and FeO abundances of Dhofar 489, we propose that a basin formed ≥4.23 Gyr ago far from the Imbrium basin and produced and metamorphosed the Dhofar 489 breccia. The discovery of spinel troctolite associated with magnesian anorthosites in Dhofar 489 suggests that these two lithologies are important components of the farside crust, and that Dhofar 489 may represent a terrain containing mixtures of deep-seated crustal rocks such as spinel troctolite and magnesian anorthosites with minor FAN-like mafic silicates. The "pure" anorthosites [42] and magnesian anorthosites [44] in the spectroscopic term could be the magnesian anorthosites with low mafic silicate abundance seen in Dhofar 489.

The Dhofar 489 mineralogy consisting of crystalline anorthositic clasts with magnesian silicates is less metamorphosed than most of the lunar magnesian granulites and offers a possibility that such rocks are important components of the farside lunar crust. The presence of such a lithology may require revision of the classical differentiation trend constructed from the Apollo samples (Fig. 10), in which the ferroan anorthosite (FAN) trend is dominant. This proposal assumes that very magnesian components in the breccias are from the spinel troctolite, which plot at the top of the HMS trend in Fig. 10.

Acknowledgements

We thank Dr. S. Yoneda at NSMT for providing us with the meteorite sample, T. Ishii and M. Otsuki at ORI for EPMA equipment, D. Garrison for support in Ar–Ar analyses, and P. Buchanan, L. E. Nyquist, K. Misawa, J. Haruyama, R. Nakamura for discussions. Financial support was provided via Grant-in-Aid for Japanese Ministry of Education, Culture, Sports, Sci. and Tech. (MEXT) (No. 15340193 to M. E., 16740297 to A. Y.). This work was carried out as a part of "Ground-based Research Announcement for Space Utilization" (PI: K. Saiki) promoted by Japan Space Forum, and partly supported by NIPR, Research Project Fund, P-8 (Evolution of the early Solar System Materials), and by the Research Forum of the Chiba Inst. of Technology. PGA was performed through the collaborative research program between universities and JAERI supported by the University of Tokyo. This work was supported in part by funds from the cooperative program (No. 005) provided by ORI, the University of Tokyo. NASA Cosmochemistry supported the Ar–Ar analysis. We also thank M. Norman and an anonymous reviewer for constructive reviews.

References

[1] D.J. Lawrence, W.C. Feldman, B.L. Barraclough, A.B. Binder, R.C. Elphic, S. Maurice, D.R. Thomsen, Global elemental maps of the Moon: the Lunar Prospector gamma-ray spectrometer, Science 281 (1998) 1484–1489.

[2] P.G. Lucey, D.T. Blewett, B.R. Hawke, Mapping the FeO and TiO_2 content of the lunar surface with multi-spectral imagery, J. Geophys. Res. 103 (1998) 3679–3699.

[3] B.L. Jolliff, J.J. Gillis, L.A. Haskin, R.L. Korotev, M.A. Wieczorek, Major lunar crustal terranes: surface expressions and crust–mantle origins, J. Geophys. Res. 105 (E2) (2000) 4197–4216.

[4] E. Gnos, B.A. Hofmann, A. Al-Kathiri, S. Lorenzetti, O. Eugster, M.J. Whitehouse, I.M. Villa, A.J.T. Jull, J. Eikenberg, B. Spettel, U. Krahenbuhl, I.A. Franchi, R.C. Greenwood, Pinpointing the source of a lunar meteorite: implications for the evolution of the Moon, Science 305 (2004) 657–659.

[5] P.H. Warren, The magma ocean concept and lunar evolution, Annu. Rev. Earth Planet. Sci. 13 (1985) 201–240.

[6] J.T. Cahill, C. Floss, M. Anand, L.A. Taylor, M.A. Nazarov, B.A. Cohen, Petrogenesis of lunar highlands meteorites: Dhofar 025, Dhofar 081, Dar al Gani 262, and Dar al Gani 400, Meteorit. Planet. Sci. 39 (2004) 503–529.

[7] R.L. Korotev, B.L. Jolliff, R.A. Zeigler, J.J. Gillis, L.A. Haskin, Feldspathic lunar meteorites and their implications for compositional remote sensing of the lunar surface and the composition of the lunar crust, Geochim. Cosmochim. Acta 67 (2003) 4895–4923.

[8] C.K. Shearer, J.J. Papike, Early crustal building processes on the moon: models for the petrogenesis of the magnesian suite, Geochim. Cosmochim. Acta 69 (2005) 3445–3461.

[9] M.M. Lindstrom, D.J. Lindstrom, Lunar granulites and their precursor anorthositic norites of the early lunar crust, J. Geophys. Res. 91 (1986) D263–D276 (Suppl.).

[10] H. Takeda, M. Miyamoto, H. Mori, S.J. Wentworth, D.S. McKay, Mineralogical comparison of the Y86032-type lunar meteorites to feldspathic fragmental breccia 67016, Proc. Lunar Planet. Sci. Conf. 20 (1990) 91–100.

[11] H. Takeda, K. Saiki, T. Ishii, M. Otsuki, Mineralogy of the Dhofar 489 lunar meteorite, crystalline matrix breccia with magnesian anorthositic clasts (abstract), Lunar Planet. Sci. XXXIV (2003) #1284 (CD-ROM).

[12] H. Takeda, D.D. Bogard, A. Yamaguchi, M. Ohtake, K. Saiki, A crustal rock clast in magnesian anorthositic breccia, Dhofar 489 and its excavation from a large basin, Lunar Planet. Sci. XXXV (2004) #1222 (CD-ROM).

[13] M. Prinz, E. Dowty, K. Keil, T.E. Bunch, Spinel troctolite and anorthosite in Apollo 16 samples, Science 179 (1973) 74–76.

[14] S.E. Haggerty, Apollo 14: subsolidus reduction and compositional variations of spinels, Proc. Lunar Sci. Conf. 3 (1972) 305–332.

[15] C.T. Herzberg, M.B. Baker, The cordierite– to spinel–cataclasitic transition: structure of the lunar crust, Proc. Conf. Lunar Highl. Crust (1980) 113–132.

[16] D.D. Bogard, D.H. Garrison, M. Norman, E.R.D. Scott, K. Keil, ^{39}Ar–^{40}Ar age and petrology of Chico: large-scale impact melting on the L-chondrite parent body, Geochim. Cosmochim. Acta 59 (1995) 1383–1399.

[17] D.H. Garrison, S. Hamlin, D.D. Bogard, Chlorine abundances in meteorites, Meteorit. Planet. Sci. 35 (2000) 419–429.

[18] D.S. McKay, D.D. Bogard, R.V. Morris, R.L. Korotev, P. Johnson, S.J. Wentworth, Apollo 16 regolith breccias:

characterization and evidence for early formation in the megaregolith. Proc. Lunar Planet. Sci. Conf. 16, J. Geophys. Res. 91 (1986) No. B4, D227–D303.
[19] S.K. Latif, Y. Oura, M. Ebihara, G.W. Kallemeyn, H. Nakahara, C. Yonezawa, T. Matsue, H. Sawahata, Prompt gamma-ray analysis (PGA) of meteorite samples, with emphasis on the determination of Si, J. Radioanal. Nucl. Chem. 239 (1999) 577–580.
[20] B.L. Jolliff, L.A. Haskin, Cogenetic rock fragments from a lunar soil: evidence of a ferroan noritic–anorthosite pluton on the Moon, Geochim. Cosmochim. Acta 59 (1995) 2345–2374.
[21] M. Ebihara, M. Honda, Distribution of rare earth elements and uranium in various components of ordinary chondrites, Meteorit. 19 (1984) 287–295.
[22] M.D. Norman, G. Ryder, Geochemical constraints on the igneous evolution of the lunar crust, Proc. Lunar Planet. Sci. Conf. 11 (1980) 317–331.
[23] B.A. Cohen, O.B. James, L.A. Taylor, M.A. Nazarov, L.D. Barsukova, Lunar highland meteorite Dhofar 026 and Apollo sample 15418: two strongly shocked, partially melted, granulitic breccias, Meteorit. Planet. Sci. 39 (2004) 1419–1447.
[24] P.H. Warren, "New" lunar meteorites: implications for composition of the global lunar surface, lunar crust, and the bulk Moon, Meteorit. Planet. Sci. 40 (2005) 477–506.
[25] J.J. Papike, G. Ryder, C.K. Shearer, Lunar samples, in: J.J. Papike (Ed.), Planetary Materials, Mineralogical Society of America, Washington, DC, 1998, pp. 5-01–5-234.
[26] J.A. Cushing, G.J. Taylor, M.D. Norman, K. Keil, The granulitic impactite suite: impact melts and metamorphic breccias of the early lunar crust, Meteorit. Planet. Sci. 34 (1999) 185–195.
[27] R.D. Warner, G.J. Taylor, K. Keil, Petrology of crystalline matrix breccias from Apollo 17 rake samples, Proc. Lunar Planet. Sci. Conf. 8 (1977) 1987–2006.
[28] D. Stöffler, H.-D. Knöll, U.B. Marvin, C.H. Simonds, P.H. Warren, Recommended classification and nomenclature of lunar highland rocks – a committee report, Proc. Conf. Lunar Highl. Crust (1980) 51–70.
[29] H. Takeda, T. Arai, A. Yamaguchi, T. Mikouchi, Important lithologies of the lunar farside crust: coarse-grained granulites or magnesian anorthosites, Lunar Planet. Sci. XXXVII (2006) #1572 (CD-ROM).
[30] K. Saiki, D. Laporte, D. Vielzeuf, S. Nakashima, P. Boivin, Morphological analysis of olivine grains annealed in an iron–nickel matrix: experimental constraints on the origin of pallasites and on the thermal history of their parent bodies, Meteorit. Planet. Sci. 38 (2003) 427–444.
[31] L.D. Raedeke, I.S. McCullum, A comparison of fractionation trends in the lunar crust and Stillwater Complex, Proc. Conf. Lunar Highl. Crust (1980) 133–153.
[32] R.L. Korotev, Section 5.2. in Chemie der Erde 65 (2005) 297–346.
[33] G.A. Snyder, L.E. Borg, L.E. Nyquist, L.A. Taylor, Chronology and isotopic constraints on lunar evolution, The Origin of the Earth and Moon, Univ. Arizona Press, 2000.
[34] F. Tera, D.A. Papanastassiou, G.J. Wasserburg, Isotopic evidence for a terminal cataclysm, Earth Planet. Sci. Lett. 22 (1974) 1–22.
[35] L.E. Nyquist, Lunar Rb–Sr chronology, Phys. Chem. Earth 10 (1977) 103–142.
[36] M.D. Norman, L.E. Borg, L.E. Nyquist, D.D. Bogard, Chronology, geochemistry, and petrology of a ferroan noritic anorthosite clast from Descartes breccia 67215: clues to the age, origin, structure, and impact history of the lunar crust, Meteorit. Planet. Sci. 38 (2003) 645–661.
[37] G. Turner, Potassium–Argon chronology of the moon, Phys. Chem. Earth 10 (1977) 145–195.
[38] W.K. Hartmann, Megaregolith evolution and cratering cataclysm models – lunar cataclysm as a misconception (28 years later), Meteorit. Planet. Sci. 38 (2003) 579–594.
[39] G. Ryder, Mass flux in the ancient Earth–Moon system and benign implications for the origin of life on Earth, J. Geophys. Res. 107 (2002) 1–14.
[40] D.D. Bogard, D.H. Garrison, L.E. Nyquist, Argon-39–Argon-40 ages of lunar highland rocks and meteorites, Lunar Planet. Sci. XXXI (2000) #1138 (CD-ROM).
[41] H. Takeda, L.E. Nyquist, H. Kojima, Mineralogical study of a gray anorthositic clast in the Yamato 86032 lunar meteorite, Lunar Planet. Sci. XXXIII (2002) #1267 (CD-ROM).
[42] D.B. Bussey, P.D. Spudis, Compositional studies of the Orientale, Humorum, Nectaris, and Crisium lunar basins, J. Geophys. Res. 105 (E2) (2000) 4235–4243.
[43] B.R. Hawke, C.A. Peterson, D.T. Blewett, D.B.J. Bussey, P.G. Lucey, G.J. Taylor, P.D. Spudis, Distribution and modes of occurrence of lunar anorthosite, J. Geophys. Res. 108 (2003) No. E6, 5050, doi:10.1029/2002JE001890, 4-1–4-16.
[44] P.G. Lucey, J. Cahill, Magnesian rock types in the lunar highlands: remote sensing using data from Lunar Prospector and Clementine, Lunar Planet. Sci. XXXVII (2006) #1660 (CD-ROM).
[45] R.L. Korotev, Geochemistry of a unique lunar meteorite from Oman, a crystalline impact-melt breccia dominated by magnesian anorthosite, Lunar Planet. Sci. XXXVII (2006) #1402 (CD-ROM).
[46] D.J. Lawrence, R.C. Elphic, W.C. Feldman, O. Gasnault, T.H. Prettyman, D.T. Vaniman, Identifying locations for future lunar sample missions, Lunar Planet. Inst. Contr. No. 1128, Moon Beyond 2002 (2002) 33.
[47] M.M. Lindstrom, S.A. Knapp, J.W. Shervais, L.A. Taylor, Magnesian anorthosites and associated troctolites and dunite in Apollo 14, breccias, Proc. Lunar Planet. Sci. Conf. 15 (1984) C41–C49.